Unpacking compaction: Effect of hydraulic pressure on alginate fouling

Citation: Tow, Emily W., and Lienhard V, John H. "Unpacking Compaction: Effect of Hydraulic Pressure on Alginate Fouling." Journal of Membrane Science 544 (December 2017): 221–233 © 2017 Elsevier B.V.

As Published: https://doi.org/10.1016/j.memsci.2017.09.010

Publisher: Elsevier

Persistent URL: http://hdl.handle.net/1721.1/111677

Version: Author's final manuscript: final author's manuscript post peer review, without publisher's formatting or copy editing

Unpacking compaction: Effect of hydraulic pressure on alginate fouling

Emily W. Tow[a,b], John H. Lienhard V[a]

[a] *Rohsenow Kendall Heat Transfer Laboratory, Department of Mechanical Engineering, Massachusetts Institute of Technology, Cambridge, Massachusetts 02139, USA*
[b] *Energy Storage and Distributed Resources Division, Lawrence Berkeley National Laboratory, Berkeley, California 94720, USA*

Abstract

High hydraulic pressure is often considered to be the cause of the high fouling propensity of reverse osmosis (RO) relative to forward osmosis (FO). Several experimental studies have shown that alginate fouling is more susceptible to cleaning in FO than in RO, but the proposal that foulant compaction causes this disparity seems to be contradicted by the incompressibility of alginate hydrogels. In addition, the effect of hydraulic pressure on fouling in osmotic membrane desalination has never been experimentally isolated, because fixed-flux comparisons at different hydraulic pressures require different draw solution osmotic pressures. In this study, a new approach to isolating the effect of hydraulic pressure on alginate fouling and cleaning is introduced: operating FO with elevated but equal feed and draw hydraulic pressures of up to 40 bar. The same concentration of sodium chloride is used as the draw solution in all trials to eliminate possible effects of draw solution composition or osmotic pressure on membrane fouling or cleaning. Theoretical modeling of the effect of alginate foulant compaction on flux reveals that foulant compaction should accelerate flux decline with low salinity feeds but retard flux decline at high salinity. However, in low-salinity alginate fouling trials, for which foulant compaction should accelerate flux decline, the measured flux decline rate was not affected by hydraulic pressure. Furthermore, when fouled membranes were cleaned by increasing the feed velocity and reducing the draw osmotic pressure, there was no apparent relationship between hydraulic pressure and cleaning effectiveness. Finally, in situ visualization of foulant removal during the cleaning process revealed no difference in foulant removal mechanisms between different hydraulic pressures. These findings demonstrate that alginate gel compaction by high feed hydraulic pressure does not occur and suggest that other explanations should be sought for FO's fouling resistance relative to RO.

Keywords: cleaning, compaction, forward osmosis, organic fouling, reverse osmosis

E.W. Tow and J.H. Lienhard V, "Unpacking compaction: effect of hydraulic pressure on alginate fouling," *J. Membrane Sci.*, **544**:221-233, 15 Dec. 2017.

1. Introduction

Forward osmosis (FO) is often compared to reverse osmosis (RO) in terms of energy consumption and fouling propensity. After some debate [1, 2], RO has been found to be more energy-efficient [3, 4, 5, 6] but also more prone to irreversible fouling [7, 8]. Although FO can foul significantly (see, e.g., [9]), some researchers have postulated that the high feed hydraulic pressure used in RO exacerbates fouling. A number of recent reports, including Refs. [7, 8, 10, 11, 12, 13, 14, 15], attribute differences between RO and FO membrane fouling to foulant compaction by high hydraulic pressure. The most compelling evidence comes from studies that show a marked difference in the effectiveness of physical cleaning between identical membranes fouled under identical hydrodynamic conditions at the same initial flux in RO and FO [7, 8, 14, 15, 16]. According to the theory that foulant cake density increases with feed hydraulic pressure, the less-compact cake layer formed near atmospheric pressure in FO should be easier to remove. However, the effects of pressure have never been experimentally isolated from other differences between FO and RO.

This study seeks to experimentally validate or invalidate the theory that high feed pressure compacts foulants. Previous studies of the effect of pressure on cleaning effectiveness in FO and RO are reviewed and the hypothetical effects of compaction on flux decline are modeled. As discussed further in Sec. 2, foulant compression is related only to feed hydraulic pressure and the pressure drop through the foulant layer and is not independently affected by the hydraulic pressure of the draw or permeate. Therefore, hydraulic pressure is experimentally isolated as an independent variable by conducting FO fouling and cleaning trials with the feed and draw streams at elevated but equal hydraulic pressures (up to 40 bar), thus sidestepping the need to vary the draw solution concentration to maintain a fixed

*Address all correspondence to *lienhard@mit.edu*

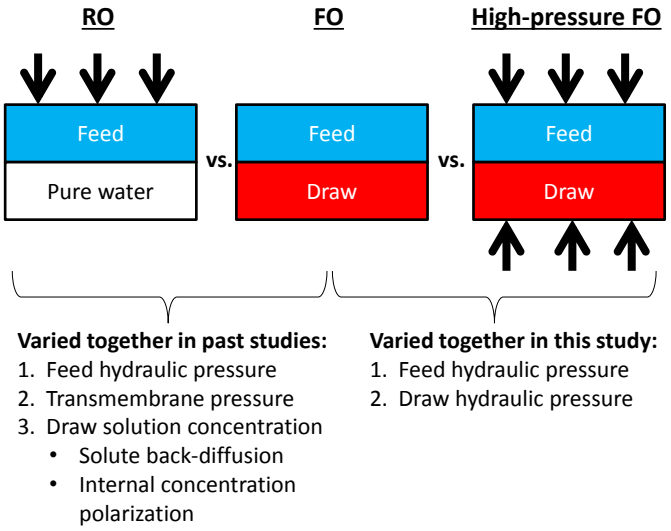

Figure 1: Methods of isolating the effect of pressure on osmotic membrane fouling taken by past studies (Refs. [7], [8], [14], and [15]) and the present study. All studies varied feed hydraulic pressure, but other variables that could potentially affect fouling were changed as well to avoid altering flux.

initial flux. Figure 1 illustrates the approaches to examining the effect of pressure on fouling taken by this study and previous studies.

To determine whether foulant compaction by high pressure significantly affects membrane fouling and cleaning, flux decline and cleaning effectiveness are measured and video is recorded of the foulant removal process at different pressures. Feed hydraulic pressure is not found to significantly affect flux decline rate, cleaning effectiveness, or foulant removal mechanisms, indicating that foulant compaction by high feed hydraulic pressure does not explain the high fouling propensity of RO relative to FO.

1.1. Definition of pressure terms

For clarity, certain terms relating to pressure are defined as follows in the context of this study: Hydraulic pressure, P, is used to mean the gauge pressure relative to atmospheric pressure. Accordingly, feed hydraulic pressure, P_f, refers to the gauge pressure of the feed. Transmembrane pressure difference (TMP) is the difference in pressure across the membrane (including any fouling layer), $P_f - P_d$, where P_d is the gauge pressure on the back side of the

membrane, whether the solution there is draw or permeate. When the draw or permeate pressure is atmospheric, as it is in RO and standard implementations of FO, feed hydraulic pressure is equal to TMP, and this distinction is unimportant. However, the present approach to testing the effect of feed hydraulic pressure on fouling propensity involves raising the hydraulic pressure of the draw solution in FO. As a result, feed hydraulic pressure is not necessarily equal to TMP in this study. The pressure drop across the foulant cake refers to the difference in hydraulic pressure between the feed solution and the feed-facing side of the membrane that results from resistance to water flow through the foulant layer. The potential effects of these various pressure differences on fouling are discussed in Sec. 2.

1.2. Literature review: role of pressure in osmotic membrane fouling

The theory that hydraulic pressure worsens fouling by compacting foulants stems from a plethora of experimental studies showing that FO fouls more slowly than RO and that FO fouling is easier to remove. The slower flux decline of FO at a given initial flux has been explained by the internal concentration polarization (ICP) self-compensation effect [17, 18, 19], which is unrelated to the system pressure. However, the lower effectiveness of cleaning fouled RO membranes is typically attributed to the high hydraulic pressure of the feed.

Multiple studies have compared fouling removal in osmotic membrane separation processes at different feed pressures and the same initial flux. Xie et al. [15] used a feed of 200 mg/L of alginate and 1 mM $CaCl_2$ and a glucose draw solution of varying concentration to compare RO, FO, and pressurized FO. Cellulose triacetate (CTA) FO membranes were used in all processes and cleaning was performed with DI water at high cross-flow velocity. Lee et al. [7] used a feed solution with 200 mg/L alginate, 1 mM $CaCl_2$, and an ionic strength of 50 mM, and cleaning was performed with the same feed at high velocity. CTA FO membranes were used with a draw solution of NaCl. Kim et al. [14] used CTA FO membranes with a feed of 100 mg/L alginate and 1 g/L of colloidal (approximately 100 nm) silica without calcium

but with 50 mM ionic strength and an NaCl draw. A stack of permeate carriers were used as a feed spacer[1] and cleaning was performed at high cross-flow velocity with the same feed solution. Mi and Elimelech [8] used CTA FO membranes with a feed solution of 200 mg/L alginate, 50 mM NaCl, and 0.5 mM $CaCl_2$ and an NaCl draw. Cleaning was performed with a solution of 50 mM NaCl at high cross-flow velocity. Alginate, a polysaccharide that complexes with calcium to form a hydrogel [20, 21], was used as a model foulant in all four studies.

Table 1 summarizes the experimental conditions and results of these four studies. Cleaning effectiveness (sometimes termed "cleaning efficiency"), which is defined as the fraction of flux lost due to fouling that is recovered by cleaning, is calculated from reported flux or normalized flux data except when cleaning effectiveness was reported. Although differences exist between the feed solutions, draw solutions, membranes, channel geometries, and cleaning methods used, all four studies varied pressure and draw concentration together to keep the initial flux fixed between trials.

Table 1: Summary of previous studies of the effect of pressure on fouling at fixed initial flux.

		Feed concentration:			Norm. flux after:			
Pressure [bar]	Draw solution	Alginate [mg/L]	Ca^{2+} [mM]	Na^{+*} [mM]	Fouling	Cleaning	Cleaning effectiveness	Ref.
0	5 M NaCl	200	1	47	0.483	0.860	0.73	[7]
31	None	200	1	47	0.681	0.681	0.00	[7]
0	4 M NaCl	200**	0.5	50	0.450	0.987	0.98	[8]
28	None	200**	0.5	50	0.500	0.730	0.46	[8]
0.0	5 M NaCl	100	0	50	0.937	0.959	0.34	[14]
18.8	3.5 M NaCl	100	0	50	0.923	0.923	0.00	[14]
0.0	2.5 M glucose	200	1	0	0.857	0.999	0.98***	[15]
5.5	1.5 M glucose	200	1	0	0.869	0.915	0.57 ***	[15]
12.5	None	200	1	0	0.840	0.843	0.02***	[15]

*Reported or calculated from ionic strength; may not include sodium added as sodium alginate.

**Also contained 1 g/L of silica colloids.

***Reported values.

[1]At least in the high-pressure trial, but possibly in both trials.

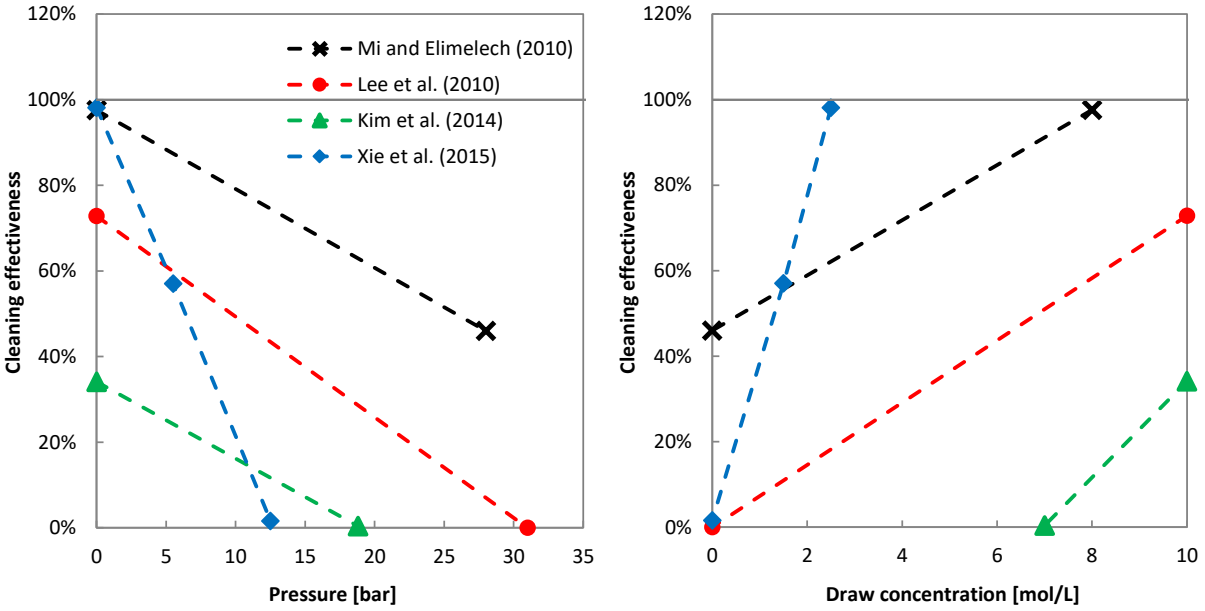

(a) Pressure (b) Concentration

Figure 2: Apparent effects of (a) feed pressure (equal to TMP in these studies) and (b) draw/permeate concentration on alginate fouling reversibility revealed by studies by Mi and Elimelech [8], Lee at al. [7], Xie et al. [15], and Kim et al. [14], in which feed pressure and draw solution concentration were varied together to maintain a particular initial flux. Points represent experimental data; dashed lines are only a guide for the eye. In cases where NaCl was the draw solute, the total ion concentration is given.

Figure 2 shows that, in this set of studies, cleaning effectiveness is not only negatively correlated with pressure but positively correlated with draw concentration. Figure 2a shows that, in each study, cleaning effectiveness decreased with increasing feed pressure. However, none of these studies truly isolated pressure as an independent variable because the concentration of the solution opposite the feed (called the "draw" in Fig. 2b, even in the case of a pure RO permeate) was also varied between these trials, as shown in Fig. 2b. Experiments in which both pressure and draw concentration are varied cannot distinguish between effects of feed hydraulic pressure, TMP, draw solute diffusion, and ICP, all of which differ between FO and RO and could potentially influence fouling, as will be discussed in in Sec. 5.

Some studies have additionally explored the physical characteristics of fouling layers formed in FO and RO both in situ and ex situ. Mi and Elimelech [8] visually examined

fouling layers formed in both processes, and found that FO fouling was more "soft and fluffy, indicating a loose structure." Fouling layers created in FO and RO have also been imaged using confocal laser scanning microscopy (CLSM) to show that both alginate cakes [15] and biofilms [22] are thinner and more uniform in RO than in FO. Although this has been considered to be evidence for foulant compaction by high pressure, the ICP self-compensation effect [17] contributes to the larger foulant thickness in FO [19]. Furthermore, no justification has yet been given for why pressure should lead to a more uniform foulant layer. Ex situ measurements and images may also be affected by changes in the gel's ionic environment that occur after the fouled membrane is removed from the experimental apparatus. Changes in calcium and sodium ion concentration within the gel, such as could occur when it is rinsed or placed in a dye solution, can cause it to shrink or swell [23]. In situ visualization of FO and RO foulant layers has also been used to compare mechanisms of foulant removal [16]. Although previous studies suggested that the low pressure in FO led to a looser foulant layer that could more easily be broken up during cleaning [7, 8], in situ observation of mechanical cleaning with reverse permeation revealed a similar progression of wrinkling, tearing, and peeling of full-thickness sheets of gel in both FO and RO [16].

Prior modeling has shown that foulant compaction by the high hydraulic pressure of the RO feed could be significant, but only for foulants with particular properties. Lay et al. [17] find the idea of compaction by high hydraulic pressure "contradictory to the well established critical flux concept," [24] which implies that, "regardless of the type of driving force, the effect of membrane fouling should be comparable under similar flux and operational conditions." However, Xie et al. [15] show through modeling that high pressure could cause compaction of compressible foulant cakes, i.e., those with Poisson's ratios less than 0.5. Xie et al. model the compression of foulants by permeate drag, which they state should affect FO and RO similarly at equal flux, as well as compression by hydraulic pressure[2], which varies

[2]Xie et al. [15] do not specify whether "hydraulic pressure" refers to the absolute feed pressure, feed gauge

between FO and RO. By modeling the foulant cake as a slab of polymer with vertical pores, they find that the ratio of compression by feed pressure ("compaction") to compression by drag is small except when the foulant is dense (when the porosity is not close to 1) or when the foulant is compressible. Although alginate was used in all trials summarized in Fig. 2, alginate gels are neither dense [25] nor compressible [26]. Xie et al. acknowledge these contradictions, but they suggest that foulant compaction by high feed hydraulic pressure could still occur because hydraulic pressure and drag "work simultaneously and therefore reinforce each other" [15]. No justification has yet been given for why a thinner, denser alginate gel should necessarily be harder to remove from a membrane.

2. Modeling the effect of compaction on flux decline

In this section, a model is developed to predict the effect of foulant compression—defined here as the fractional reduction in volume of a unit mass of foulant solids (e.g., alginate polymer)—on permeate flux. First, the roles of feed hydraulic pressure, TMP, and pressure drop through the foulant layer are briefly discussed. Next, in Sec. 2.1, a model is developed to predict the hypothetical effect of compression by hydraulic pressure on flux decline in FO. Finally, in Sec. 2.2, the model is evaluated to aid in the interpretation of experimental results.

High feed hydraulic pressure has the potential to reduce the volume of compressible foulants. The volume per unit mass of foulant depends on the gel's bulk modulus and the hydraulic pressure on the feed side of the membrane, where the foulant cake is located. The ratio between the volume of a particular mass of alginate polymer under high pressure to

pressure with respect to atmosphere, or TMP, but it is presumed that the intended meaning is feed gauge pressure with respect to atmosphere because their derived expression would predict no foulant compression at zero flux and atmospheric feed pressure. Gauge pressure of the feed with respect to atmosphere is equal to TMP in standard RO, FO, and pressure-assisted FO processes (the processes tested by Xie et al.), because the draw or permeate is maintained at atmospheric pressure. However, this distinction is important when interpreting the theory developed by Xie et al. in the context of the present study, which includes trials at elevated gauge pressure but zero TMP.

the volume of the same mass of alginate at atmospheric pressure can be calculated using the definition of the bulk modulus, K, and its relationship to the compressibility, ν, and Young's modulus, E, of the alginate gel (see Ref. [27]) using Eq. 1, which assumes small displacements:

$$\frac{V}{V_u} = 1 - \frac{P}{K} = 1 - \frac{3P(1-2\nu)}{E}, \tag{1}$$

where V is the volume of the cake, V_u is the uncompressed volume the same cake at atmospheric pressure, and P is the gauge pressure (with respect to atmosphere) of the feed. More compressible foulants, for which ν is significantly less than 0.5, will experience greater compression in response to increased feed hydraulic pressure.

Equation 1 shows that foulant compressibility ($\nu < 0.5$) is necessary for feed pressure to affect foulant volume (i.e., for compaction to occur). Values of E and ν for alginate gel, the model foulant used in studies that saw a difference in fouling reversibility between FO and RO, as described in Sec. 1.2, have been calculated by Wang et al. [26] from micro-sphere compression tests conducted at high compression speed to minimize flow of water out of the nanoporous gel. Wang et al. show that alginate is incompressible or nearly so, and it is therefore unlikely that high hydraulic feed pressure will contribute to compressing alginate foulant. Nevertheless, the dominant explanation of RO's high fouling propensity relative to FO is that high feed hydraulic pressure compacts foulants, so he present model considers the possibility that alginate gel could be slightly compressible and thus its volume (per unit mass of polymer) could decrease with increasing feed hydraulic pressure.

According to Eq. 1, incompressible ($\nu = 0.5$) foulants will not be compressed by high feed hydraulic pressure. However, because most membrane foulants are bicontinuous mixtures of solids and liquid water, the drag force exerted by flowing water on the solid matrix can deform the foulant even if the mixture (in this case, alginate gel) is incompressible. Thus, as shown by Xie et al. [15], even incompressible foulants can undergo volumetric compression if the

flow of water through the foulant's fine pore structure causes a hydraulic pressure drop across the cake.[3] To distinguish between these two causes of foulant compression, compression due to high feed pressure will be referred to as "compaction," while compression due to drag will be referred to as "drag-induced compression."

Taken independently from flux and feed hydraulic pressure, TMP itself is unlikely to cause compression of foulants on FO or RO membranes because of their sub-nanometer pores [28]. Fouling and cleaning could theoretically be affected by TMP in the case of single-layered nanoporous graphene RO membranes (see, e.g., Ref. [29]), which have straight-through pores, but the active layers of commercial RO and FO membranes are generally considered to be either nonporous or composed of an interconnected nano-pore network. The solution-diffusion model [30, 31] considers the active layer to be nonporous and, modeling the active layer and contained water as a single phase [32], predicts uniform pressure equal to that of the feed throughout the active layer. According to this model, foulants on the feed side of the membrane are only exposed to the feed pressure and the permeate (or draw) pressure is irrelevant. More recent studies show that the RO active layer contains free-volume holes with diameters in the range of 0.40-0.58 nm [28]. Even so, as long as water flow paths are interconnected (as they are in most porous materials), pore blocking should not lead to propagation of the draw/permeate pressure back to a foulant particle deposited on the feed side, and the draw/permeate pressure (and thus TMP) should again be irrelevant. However, TMP may still affect fouling and cleaning in other ways, as discussed further in Sec. 5.1. The present study does not vary TMP, and thus cannot resolve effects of TMP on fouling.

[3]Even in FO, when the feed and draw solutions are both at atmospheric pressure, a pressure drop can exist across the foulant layer: As water is pulled through the active layer of a fouled membrane by osmosis, the pressure at the foulant–membrane interface dips below atmospheric so that the pressure gradient in the foulant layer is large enough to overcome resistance to flow through the nanoporous gel.

2.1. Properties of compressed foulant cakes

Flux in FO depends on the thickness, tortuosity, porosity, and hydraulic diameter of the foulant layer as well as the feed composition, draw composition, channel hydrodynamics, and membrane properties [19]. The model developed here assumes that only the foulant layer properties are affected by hydraulic pressure, and neglects any possible effects of pressurization on the membrane or solutions. The model focuses on alginate fouling because of the extensive use of alginate in previous studies of the effect of pressure on fouling as well as the structural similarity of alginate to microbial extracellular polymeric substances (EPS) [33], which play a significant role in biofouling [34]. To relate changes in the foulant layer properties to volumetric compression, the alginate gel is modeled as an isotropic 3–D scaffold of alginate chains in water with a uniform pore size. The surface area of the polymer–water interface is assumed to be a function of the ionic composition of the surrounding solution and thus constant during compression. The equations developed in this section are intended to predict the effect of compression on foulant cake properties regardless of whether compression occurs due to permeation through the foulant cake, high feed hydraulic pressure, or both.

The alginate gel pore hydraulic diameter, D_h, can be defined on a volumetric basis as it would be for a tube bundle:

$$D_h = \frac{4V\phi}{A_s} \tag{2}$$

where A_s is the alginate–water interfacial surface area inside a volume V of gel, and ϕ is the gel porosity (or water volume fraction). Assuming the alginate chains are not themselves compressible and volume reduction occurs only due to outflow of water, the volume of polymer should be constant during the compression:

$$(1-\phi)V = (1-\phi_u)V_u, \tag{3}$$

where the subscript u refers to the uncompressed gel at atmospheric pressure. Substituting Eq. 3 into Eq. 2 gives the hydraulic diameter as a function of volumetric compression:

$$D_h = D_{h,u}\Big(1 - \frac{1 - V/V_u}{\phi_u}\Big), \tag{4}$$

where $D_{h,u} = 4V_u\phi_u/A_s$ is the gel hydraulic diameter at atmospheric pressure. Equation 4 shows that pore hydraulic diameter decreases due to compression, in agreement with the assessment of Xie et al. [15].

The gel porosity decreases with compression according to Eq. 5:

$$\phi = 1 - \frac{(1 - \phi_u)V_u}{V}. \tag{5}$$

The relationship between porosity and tortuosity, τ, has been the subject of many investigations, some of which are reviewed in Ref. [35]. A general correlation for packed beds of various geometries is given by Mauret and Renaud [36]:

$$\tau = 1 - 0.49\ln(\phi). \tag{6}$$

Due to the high porosity typical of alginate gels, tortuosity is expected to remain close to one.

Compression is typically thought to accelerate flux decline, but foulant compression may either increase or decrease flux decline rate depending on the dominant driver of flux decline. Although the thickness, δ, of a gel containing a fixed mass of polymer decreases due to compression as in Eq. 7,

$$\delta = \delta_u \frac{V}{V_u}, \tag{7}$$

the simultaneous decrease in pore size causes an overall increase in hydraulic resistance, which is proportional to δ/D_h^2 [19]. On the other hand, cake-enhanced concentration polar-

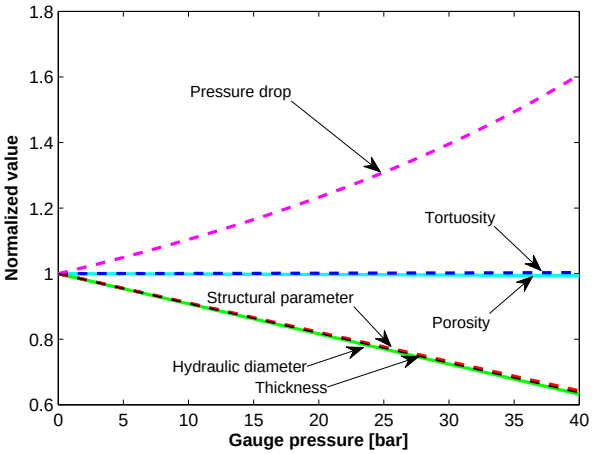

Figure 3: Modeled effect of pressure on foulant cake properties with a hypothetical Poisson's ratio of $\nu = 0.495$. Each parameter is normalized by its uncompressed value for a cake formed at atmospheric pressure.

ization (see, e.g., [37]) is reduced as a result of the decreased cake thickness. Both mechanisms of flux decline are also affected by changes in porosity and tortuosity resulting from compaction, although the high porosity of alginate gel renders these effects insignificant.

The modeled effect of compression on the cake properties D_h, ϕ, τ, and δ, as well as the cake's structural parameter ($\delta\tau/\phi$) and hydraulic pressure drop at a given flux (see [19]) is plotted in Fig. 3 for a hypothetical 2% wt. alginate gel with a slight compressibility ($\nu = 0.495$). Pressure drop through the foulant cake increases while thickness, cake structural parameter, and pore hydraulic diameter decrease almost identically. Tortuosity and porosity change very little because of alginate's high water mass fraction.

2.2. Foulant accumulation and flux decline

The model developed in this section incorporates the compression-induced changes in foulant layer properties modeled in the previous section with a deposition–minus–removal model of foulant accumulation to predict the effect of foulant compression on flux decline.

Foulant accumulation on the membrane is modeled as the difference between deposition and removal rates as in the critical flux model for cake fouling developed for microfiltration

by Field et al. [24] and validated against RO fouling experiments by Qureshi et al. [38]. Various mechanisms govern transport toward and away from the membrane, depending on the separation process and the type of foulant. For the alginate fouling of FO membranes considered here, foulant deposition rate is modeled as being equal to the rate of convection toward the membrane, which is proportional to the permeate flux J_w and foulant mass concentration $\rho_{A,f}$ (in kg alginate/m^3 feed) in the feed:

$$\dot{m}_D'' = J_w \rho_{A,f}. \tag{8}$$

Foulant removal rate is assumed to be constant in time, as in the cake filtration model of Field et al. [24]. In RO, the removal rate is reported to be a function of solution composition and temperature, cross-flow velocity, system geometry (e.g., feed channel thickness and spacer type), and TMP [38]. Here, the same is assumed to be true for FO, and therefore the rate of removal is not expected to vary between the FO trials conducted in this study under conditions that are identical except for the varying feed hydraulic pressure. Over time, flux is expected to approach an asymptote at which the rate of deposition equals the rate of removal (the "critical flux" [24]), or at least reduce to a level where further foulant accumulation is negligible (the "threshold flux" [39]). Given that neither rate of deposition nor rate of removal are expected to depend on hydraulic pressure, the asymptotic flux is not expected to vary with hydraulic pressure. The pressure-independence of the asymptotic flux, J_w^*, has been demonstrated experimentally in a comparison of alginate fouling in FO, pressurized FO, and RO with identical membranes, in which the flux reached an asymptotic limit of approximately 14 L/m^2-hr (lmh) in all three cases despite differing pressures [15].

The net accumulation rate of foulant mass on the membrane, $\dot{m}''$, is equal to the rate of deposition minus the rate of removal, where the rate of removal is equal to the rate of

deposition evaluated at the asymptotic flux, J_w^*:

$$\dot{m}''_{\text{net}} = (J_w - J_w^*)\rho_{A,f}. \tag{9}$$

Given the very low permeate recovery (<1%) of a single pass through the 8 cm-long channel used in the present experiments, the water flux and foulant mass flux are assumed to be uniform. Effects of spatial variations in mass transfer coefficient on flux and foulant removal rate are neglected in the present analysis.

The rate of change in foulant cake thickness is related to the foulant accumulation rate and gel porosity:

$$\frac{\mathrm{d}\delta}{\mathrm{d}t} = \frac{\dot{m}''_{\text{net}}}{(1-\phi)\rho_A} = \frac{[J_w(t) - J_w^*]\rho_{A,f}}{(1-\phi)\rho_A}, \tag{10}$$

where ρ_A is the density of the alginate polymer that composes the solid phase of the gel.

Foulant thickness and flux decline can be predicted by integrating Eq. 10 numerically: At each time step, flux is calculated as a function of foulant thickness and morphology using the layered model of water and solute transport through fouled FO membranes detailed in Ref. [19], which accounts for both cake-enhanced osmotic pressure and cake hydraulic resistance, and then the change in foulant layer thickness is calculated using Eq. 10.

Depending on foulant composition and feed salinity, compression can lead to either higher or lower rates of flux decline. In Fig. 4, the initial rate of flux decline is predicted as a function of feed salinity for several degrees of volumetric compression. The feed solution is modeled as 0.02% wt. alginate and 1 mM $CaCl_2$ as in the experiments reported in Sec. 4. The draw solution is modeled as 5 M NaCl. The pore hydraulic diameter of the uncompressed foulant cake[4] is modeled using a linear interpolation of pore diameters estimated from experimental measurements at different NaCl concentrations in Ref. [19] for alginate cakes formed in

[4]Calculations from experimental data [19] suggest that pore diameter rises from approximately 6 nm at 10 mM NaCl to 20 nm at 390 mM NaCl, at which point hydraulic resistance becomes negligible in comparison to cake-enhanced osmotic pressure.

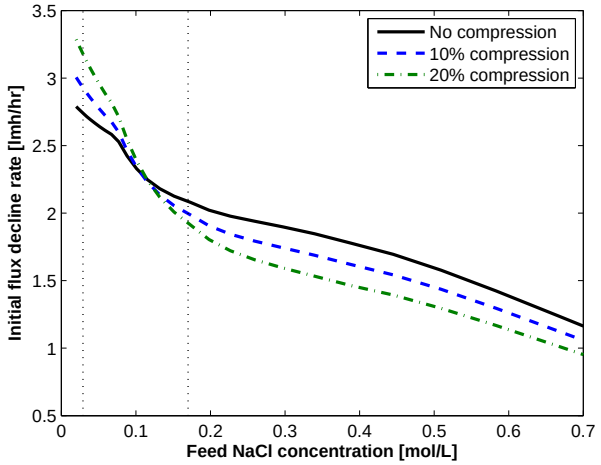

Figure 4: Predicted initial flux decline rate as a function of feed NaCl concentration and alginate gel strain due to three hypothetical degrees of compression (including none). The feed solution is modeled as 0.02% wt. alginate and 1 mM $CaCl_2$ and the draw solution is modeled as 5 M NaCl. The NaCl concentrations of the two solutions tested experimentally in this paper (29 and 174 mM) are marked with vertical dotted lines.

feed solutions containing 1 mM $CaCl_2$. The alginate polymer density was assumed to be $\rho_A = 1800$ kg/m^3 [25] and the uncompressed gel porosity was estimated to be $\phi_u = 0.9889$ based on a polymer mass fraction of 2%, which is within the typical range of alginate gels [25]. The asymptotic flux, at which the rate of foulant advection equals the rate of removal, is taken to be 11 lmh based on experimental measurements under the modeled conditions. FO membrane properties, which themselves affect flux decline, are based on the present authors' previous measurements of HTI's CTA membranes [19] and are assumed to be independent of pressure; this assumption is supported by measurements of the initial flux before fouling (Fig. Appendix A), which show no effect of pressure on unfouled membrane performance.

Figure 4 shows that the effect of alginate compression on flux decline depends on NaCl concentration. At low NaCl concentration, compression should increase the initial rate of flux decline. However, at higher NaCl concentration, the higher feed osmotic pressure and foulant pore diameter cause the reduction in cake-enhanced osmotic pressure to overcome the increase in hydraulic drag, and the effect of compaction is actually to *mitigate* flux

decline.

The theoretical prediction that cake compression should raise the rate of flux decline at 29 mM NaCl will be used to interpret experimental results and determine whether or not foulant compaction by high feed hydraulic pressure occurs. If the flux decline rate at a given flux increases with increasing feed hydraulic pressure at 29 mM NaCl, it will be concluded that foulant compaction by high feed hydraulic pressure occurs. If flux decline rate is independent of pressure, it will be concluded that alginate fouling is (as direct measurements of alginate gels [26] suggest) incompressible and that foulant compaction by high feed hydraulic pressure does not occur.

3. Experimental methods

The effect of hydraulic pressure on FO membrane fouling was tested in a custom plate-and-frame FO membrane module that could be pressurized equally on feed and draw sides. Pressure, temperature and flow rate were controlled while changes in flux were measured. Each flow channel was 80 mm long, 30 mm wide, and 1 mm deep. The experimental apparatus is shown schematically in Fig. 5; details of measurement, control, and module design are given in Refs. [16, 19]. In situ visualization of foulant removal is enabled by a polycarbonate window in the membrane module (see Ref. [16] for details). Feed and draw pressures are kept equal by connecting the back pressure regulators (Equilibar) in both feed and draw loops to the same pressure-regulated supply of nitrogen gas.

Whereas previous comparisons pressurized only the feed stream [7, 8, 14, 15] and varied draw solution concentration to achieve a fixed initial flux, this apparatus allows feed and draw pressures to be raised together, eliminating the need to vary the draw solution concentration. It also separates feed hydraulic pressure from TMP; by varying the feed and draw pressures together, TMP can be maintained close to zero, as is typical in FO systems.

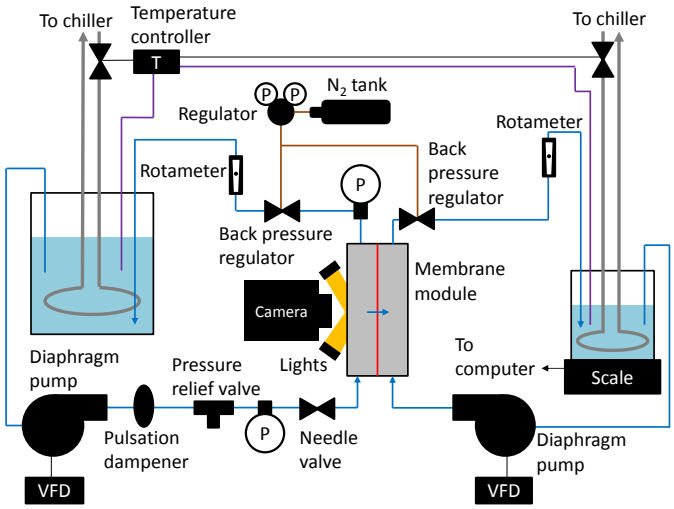

Figure 5: Schematic diagram of the experimental high-pressure FO fouling measurement apparatus. Feed and draw streams are pressurized equally. Figure adapted from Ref. [16].

3.1. Feed and draw solutions

The feed solution contained deionized water, 200 mg/L sodium alginate (Sigma-Aldrich A2033, referred to as "alginate" elsewhere in this report), 1 mM calcium chloride (Alfa Aesar 99% min.) to induce gelation of alginate, and varying concentrations of sodium chloride (Alfa Aesar 99% min.). The sodium chloride concentration was varied in order to capture effects of both cake-enhanced concentration polarization and cake hydraulic resistance. In some trials, 7.6 μM methylene blue (Alfa Aesar), which was previously shown to be a benign dye that does not affect fouling rate or cleaning effectiveness in RO [16], is used in the feed to dye the alginate gel for visualization of foulant removal.

A nearly-saturated sodium chloride solution (approximately 5 M) in deionized water was used as the draw solution at a cross-flow velocity of 4.3 cm/s. The draw solution was partially degassed before use to prevent accumulation of air in the draw loop and associated flux measurement error. The highly-concentrated draw, though not practical for real FO desalination systems, was used in this experiment to drive a high water flux (similar to fluxes used in RO) and accelerate fouling.

3.2. Membranes and spacers

Asymmetric cellulose triacetate (CTA) membranes (Hydration Technology Innovations) were used with the active layer facing the feed. Properties of these membranes were previously characterized in Ref. [19]. Membranes were soaked in a solution of 50% ethanol and 50% deionized water for approximately 5 minutes and then rinsed in deionized water before being installed in the membrane module. They were then equilibrated with foulant-free feed and draw solutions (with feed velocity at least 16.7 cm/s during equilibration to discourage premature fouling) at the final pressure for at least 90 minutes and until flux stabilized.

Two layers of 0.43 mm-thick spacer (Sterlitech 17 mil) were used to maintain the draw channel at the appropriate depth and increase the mass transfer coefficient. Where noted, one 0.79 mm-thick spacer (Sterlitech 31 mil) was used in the feed channel to reduce the rate of fouling. The higher velocity of the feed relative to the draw created a slight pressure difference between the feed and draw channels such that the membrane lay flat against the draw spacers.

3.3. Fouling and cleaning procedures

After equilibrating the membranes with the draw solution and foulant-free feed, concentrated alginate and calcium chloride solutions were added sequentially and the feed velocity was reduced from 16.7 cm/s to 8.3 cm/s to initiate fouling. Fouling was carried out for 8 h before cleaning.

During the cleaning step, the feed cross-flow velocity was increased by a factor of three to 25 cm/s and osmotic backwashing was carried out for 60 minutes. In this case, osmotic backwashing involved substituting Cambridge, Massachusetts tap water (which is acceptable to use with the chlorine-tolerant CTA membranes) in place of the draw solution so that the direction of permeation reversed. Permeation direction was reversed to enhance cleaning by both changing the direction of the viscous drag force and changing the ionic composition of

the solution within the gel to encourage swelling and gel detachment [16]. After 60 minutes, the feed velocity was returned to 8.3 cm/s, the draw solution was re-introduced, and the draw tank salinity was re-measured to account for any water added during the transition from the cleaning step. Pressure was maintained throughout the entire cleaning step at the value used during the fouling period.

Fouling and cleaning trials were repeated three times under each of six sets of conditions. In six trials (one under each set of conditions), video of the fouled membrane was recorded during the cleaning process. Videos are provided in the supplementary materials.

4. Results

4.1. Flux decline

In this section, rates of flux decline are compared across trials at different pressures, demonstrating the absence of anticipated effects of compaction on flux decline. Although the experimental design aimed to decouple feed hydraulic pressure from flux, significant variation in initial flux occurred. However, there was no correlation between initial flux and feed pressure (see Appendix A). To account for the effects of initial flux on fouling and flux decline, the measured flux data (Fig. 6 and 9) are presented along with the relationship between flux decline rate and flux (Figs. 7 and 10).

Figure 6 shows measured flux decline for three trials each at 0, 4, 20, and 40 bar with a feed solution of 29 mM NaCl, 1 mM $CaCl_2$, and 200 mg/L alginate, without a feed spacer[5]. Repeated trials are denoted by symbols of the same shape and outline color with different fill colors. The gap after 8 h is the cleaning step; cleaning effectiveness is discussed in Sec. 4.2.

The theory developed in Sec. 2 predicts that, for the low-salinity trials shown in Fig. 6, cake-enhanced osmotic pressure is negligible and foulant compaction should lead to faster

[5]An earlier subset of the data shown in Fig. 6 are reported in Ref. [41] by the same authors.

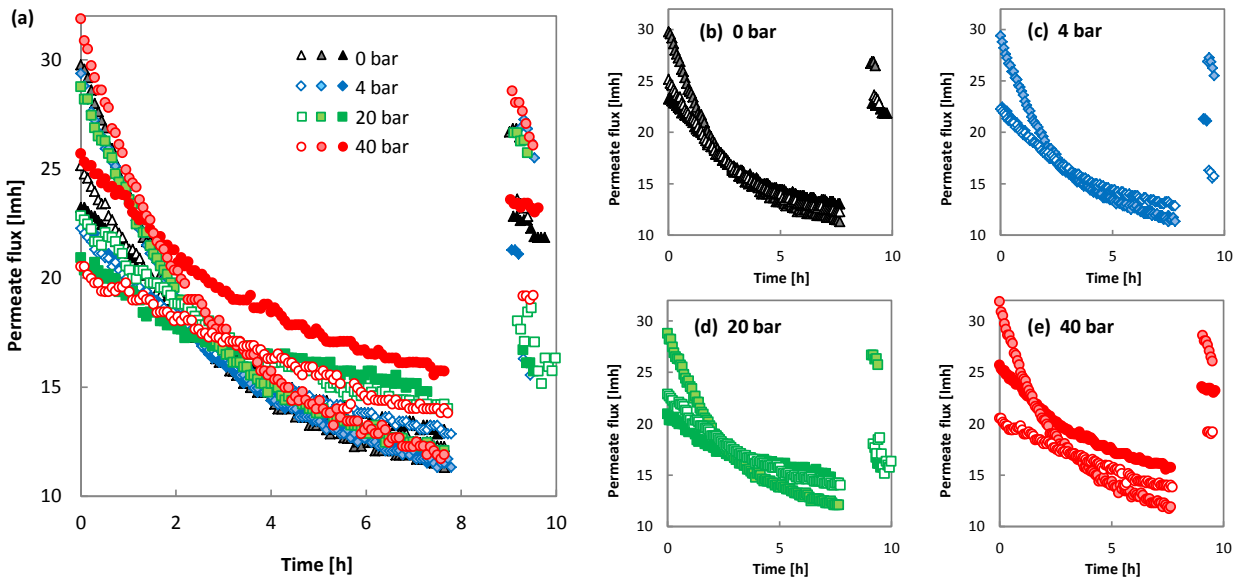

Figure 6: Experimental flux decline curves for FO fouling at various pressures with a low-salinity feed (29 mM NaCl, 1 mM $CaCl_2$, and 200 mg/L alginate) and no feed spacer: (a) all data and (b–e) data plotted separately by pressure. Trials repeated under identical conditions are denoted by symbols of the same shape and outline color.

flux decline at higher pressure due to the increase in hydraulic resistance of a more dense fouling layer. However, no effect of pressure is apparent. Trials with higher initial flux generally exhibit more rapid flux decline, and the flux decline profiles of most trials cross around 3 h. The four trials (one at each of the four pressures) that began at high flux (28–32 lmh) and used membranes cut from the same membrane sheet exhibit nearly identical flux decline profiles, suggesting that hydraulic pressure lone does not affect flux decline.

To untangle the effects of pressure, flux, and initial flux, flux decline rate (calculated over 2 h periods) is plotted versus flux in Fig. 7. Data marker shapes correspond to operating pressure and colors correspond to initial flux range. The relationship between flux decline and flux is roughly linear due to the convection of foulants to the membrane [38]. No correlation is evident between pressure and flux decline rate. When data is compared to other trials with the same initial flux in Fig. 7b–e, flux decline rate is largely a function of flux. In Fig. 7d, the trial at 40 bar exhibited significantly lower rates of flux decline than

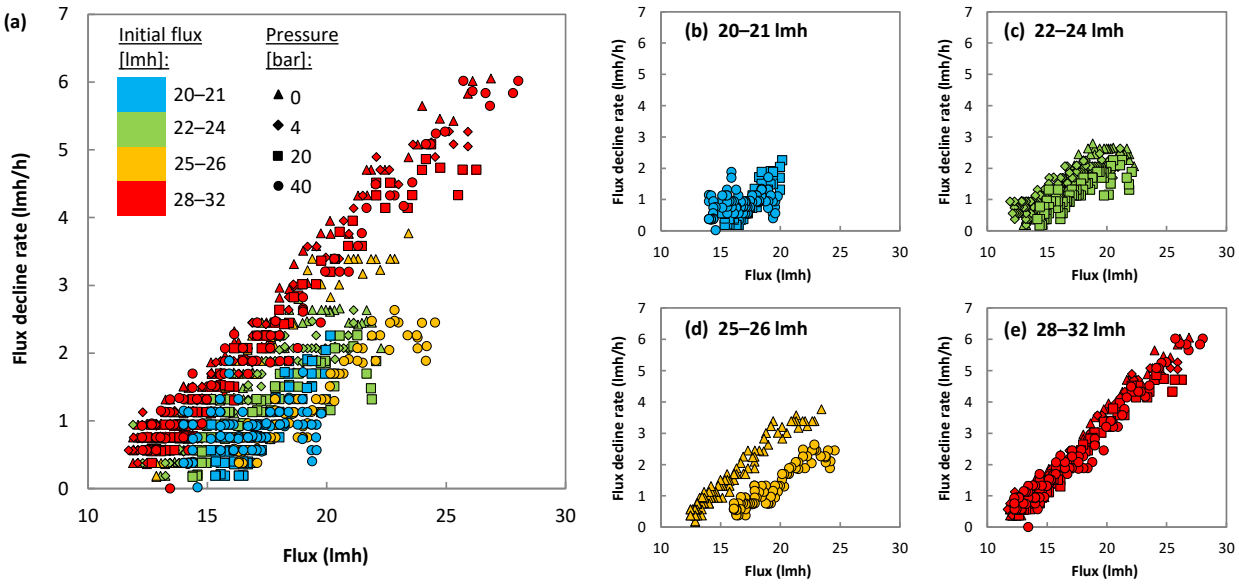

Figure 7: Flux decline rate (averaged over 2 h) plotted against flux for the low-salinity data shown in Fig. 6: (a) all data and (b–e) data grouped by initial flux. Symbol shape denotes operating pressure; color denotes initial flux. Flux decline rate at a given flux generally increases with increasing initial flux for this low-salinity feed.

the trial at 0 bar, which cannot be explained by foulant compaction because compaction by high hydraulic pressure should raise the rate of flux decline with this low-salinity feed. Overall, higher initial flux appears to lead to a higher flux decline rate at any given flux.

The dependence of flux decline rate on not only the current flux but also the initial flux can be explained by considering the effects of further foulant accumulation on the existing foulant cake, as illustrated in Fig. 8(a–b). When additional gel forms on the surface of existing gel, it creates additional drag and increases the pressure drop through the gel, compressing the existing gel. As discussed in Sec. 2, porous gels can be compressed due to the drag-induced pressure difference across the gel layer, which increases as new gel is deposited. When the gel pore size and feed salinity are low enough that compression accelerates flux decline (as in the case of the low-salinity trials in Fig. 7), then the rate of flux decline at a given flux should increase with initial flux, as it seems to in Fig. 7.

Model predictions further support the theory that drag-induced compression enhances

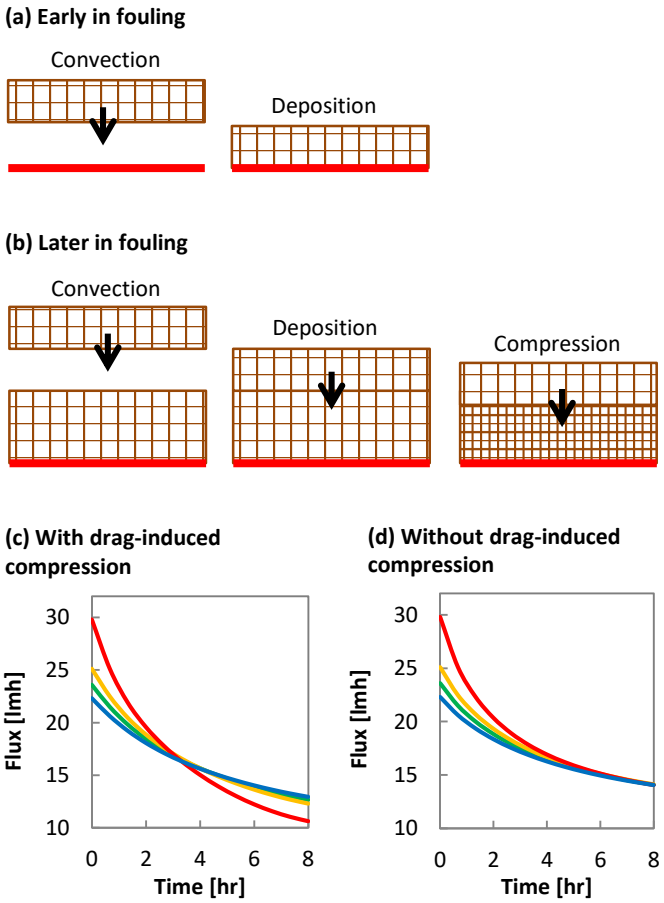

Figure 8: Effect of drag-induced compression on flux decline: (a) When little to no fouling has occurred, the pressure drop across the foulant cake is negligible, and so cake compression by drag is negligible. (b) When foulant deposits on top of existing foulant, it increases the drag-induced pressure drop across the cake, leading to foulant compression (regardless of feed hydraulic pressure or TMP). (c–d) Theoretical flux decline curves for a low-salinity feed (29 mM NaCl, 1 mM $CaCl_2$, and 200 mg/L alginate) with and without the effect of drag-induced compression, respectively; note the crossing of flux decline curves in (c).

flux decline at low salinity regardless of operating pressure. When cake compression is modeled as proportional to only the drag-induced hydraulic pressure drop[6] across the cake (as in the model of Xie et al. [15], but using a Poisson's ratio of $\nu = 0.5$ to represent an incompressible foulant) with a low-salinity feed, the flux decline curves of FO fouling trials beginning at different initial fluxes cross, as shown in Fig. 8c. When drag-induced compression is neglected, flux decline curves of membranes with different permeabilities converge, but do not cross (Fig. 8d). The experimental measurements of fouling with a low salinity feed do exhibit crossing of flux decline curves (see Fig. 6) as predicted when drag-induced compression is accounted for.

To more accurately simulate membrane fouling in real desalination systems, the effect of pressure on fouling was also tested using a feed spacer and a more saline feed solution (174 mM NaCl, 1 mM $CaCl_2$, and 200 mg/L alginate)[7]. With this feed solution, the model of Sec. 2 shows that both hydraulic resistance and cake-enhanced concentration polarization should contribute to flux decline, and the net effect of compaction is expected to mitigate flux decline, but only slightly (refer to Fig. 4). No independent effect of pressure on flux decline rate is discernible from flux measurements (Fig. 9).

The effect of pressure, flux, and initial flux on flux decline rate are presented in Fig. 10 for the trials using the moderate-salinity feed solution (174 mM NaCl, 1 mM $CaCl_2$, and 200 mg/L alginate) and a feed spacer. As in Fig. 7, symbol color and shape correspond to hydraulic pressure and initial flux, respectively. Flux decline rate clearly increases with increasing flux, but there is no clear relationship between flux decline rate and pressure or initial flux. This is expected, as the effect of compression on flux (due to either drag or high feed hydraulic pressure) should be minimal for alginate fouling with this feed composition.

[6]Pressure drop calculated using the cake hydraulic resistance model and cake pore diameters interpolated from data in Ref. [19]).

[7]Flux data for one trial at atmospheric pressure was also presented in comparison with a spacer-free trial in the present authors' previous report [16].

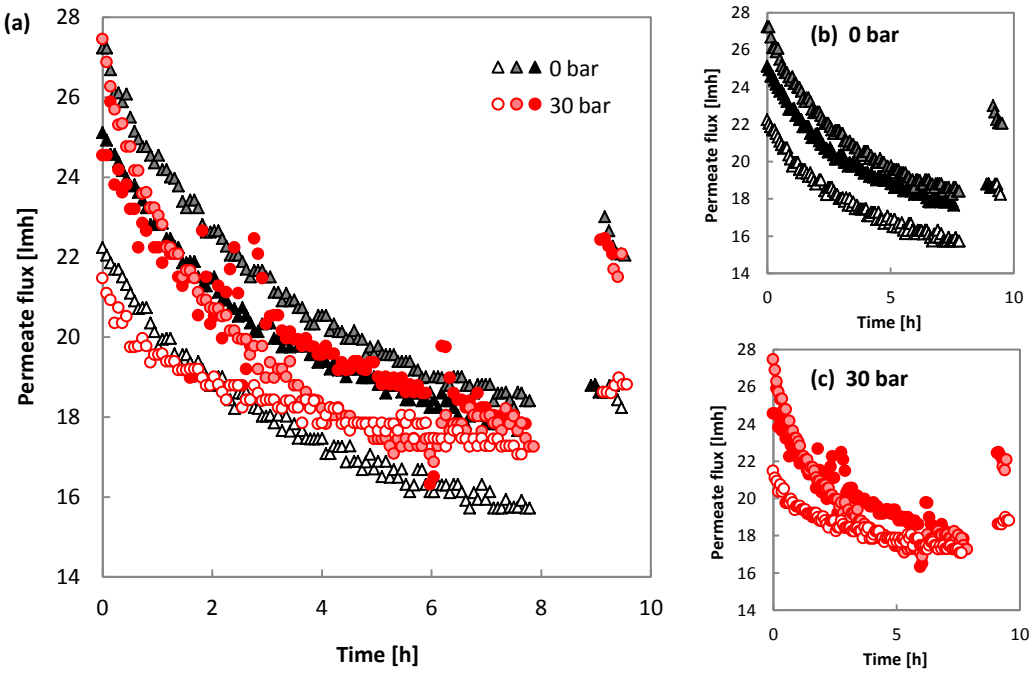

Figure 9: Experimental flux decline curves for FO fouling with a feed spacer at various pressures with a moderate-salinity feed (174 mM NaCl, 1 mM $CaCl_2$, and 200 mg/L alginate): (a) all data and (b–c) data plotted separately by pressure. Repeated trials are denoted by symbols of the same shape and color.

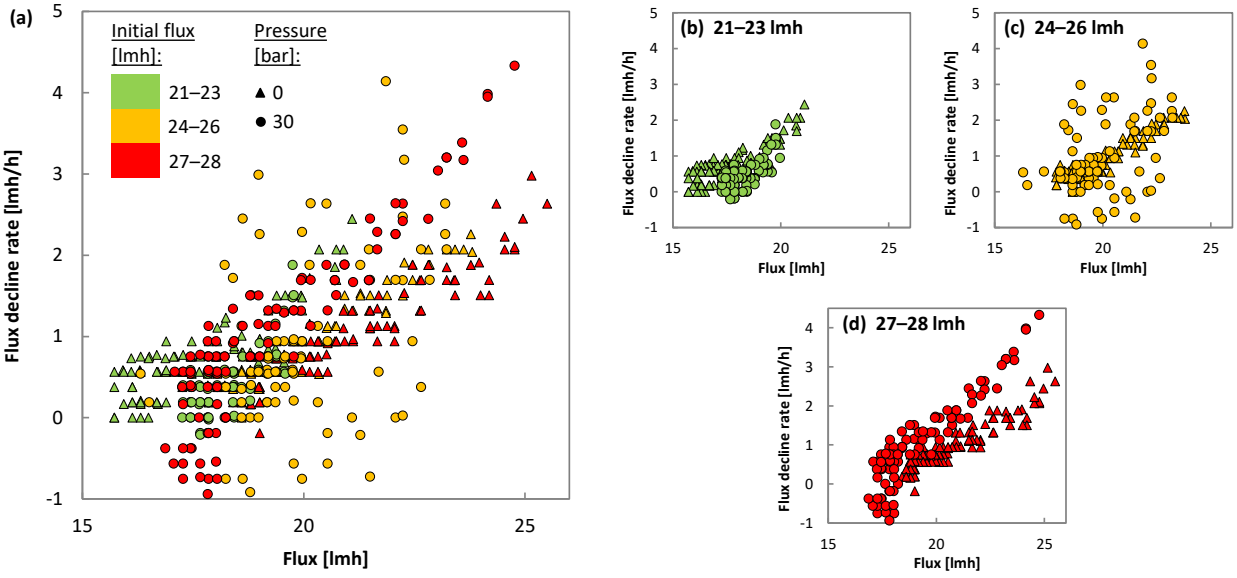

Figure 10: Flux decline rate (averaged over 2 h) plotted against flux for the moderate-salinity data shown in Fig. 9: (a) all data and (b–d) data grouped by initial flux. Symbol shape denotes operating pressure; color denotes initial flux.

The dependence of flux decline rate on initial flux at low salinity (and lack thereof at moderate salinity) shows that these experiments can capture the effect of foulant compression on flux; however, the dependence of flux decline rate on initial flux is only due to drag-induced compression. The lack of a discernible effect of feed hydraulic pressure on flux decline rate at low salinity (Fig. 7), where foulant compression should accelerate flux decline, shows that feed hydraulic pressure did not significantly compact foulants.

4.2. Cleaning effectiveness

Even though the fouling trials in Sec. 4.1 did not demonstrate the expected effect of foulant compaction on flux decline, previous studies have shown substantial disparities in cleaning effectiveness between FO and RO fouled at the same initial flux under identical hydrodynamic conditions. Therefore, this section examines the effect of pressure on the effectiveness of foulant removal.

Figure 11 shows the calculated cleaning effectiveness (defined in Appendix B) for all experimental trials. Significant variability in cleaning effectiveness occurs even under replicated conditions, which is not surprising, given the large size of sloughed alginate gel pieces (see Fig. 12). Due to the peeling mechanism of gel removal by osmotic backwashing, the cleaning effectiveness is almost binary in the absence of feed spacers. With feed spacers, the gel breaks into much smaller pieces (roughly the size of the spacer grid; see Ref. [16]), and the average cleaning effectiveness was closer to 50% at both 0 and 30 bar.

Figure 11 does not reveal a negative effect of pressure on fouling reversibility. Correlation coefficients between pressure and cleaning effectiveness were -0.04, 0.54, and 0.13 for the low salinity data, moderate salinity data, and all data, respectively, demonstrating the lack of a negative correlation between pressure and cleaning effectiveness when pressure is isolated. Cleaning was consistently effective at 40 bar, the highest pressure tested, demonstrating that low pressure is not a requirement for effective membrane cleaning. Contrasting the significant difference in fouling reversibility between RO and FO identified by previous studies (Fig. 2)

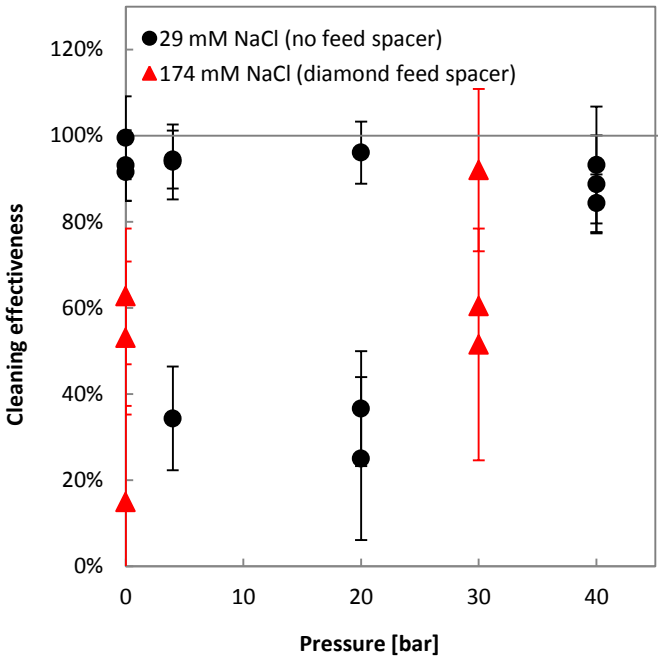

Figure 11: Cleaning effectiveness as a function of pressure for all trials shown in Figs. 6 and 9. Error bars represent 95% confidence intervals calculated as described in Appendix C.

with the relative indifference to pressure demonstrated in Fig. 11, it would appear that the cause of the superior fouling reversibility of FO is something other than its low pressure.

Because previous reports [7, 8] have postulated that feed pressure affects cleaning effectiveness by altering the mechanism of foulant removal, the cleaning process was recorded on video for one trial at each pressure and salinity tested. The six videos are available in the supplementary materials. The foulant removal process is clearly visible in the low-salinity trials without a feed spacer, so stills at key points (before, during, and after the foulant layer peels off) are provided in Fig. 12. Without a spacer, the mechanism of foulant removal is consistent across feed pressures from 0–40 bar: The foulant layer wrinkles, stretches, tears, and then completely detaches from the membrane.[8] In the moderate-salinity trials with a feed spacer, the feed spacer obscures visibility somewhat, so still images are not included

[8]The same behavior was observed in RO as well as FO in the present authors' previous in situ visualization study [16] and can be explained by alginate gel swelling due to reduction in ion concentration in the gel during the cleaning step.

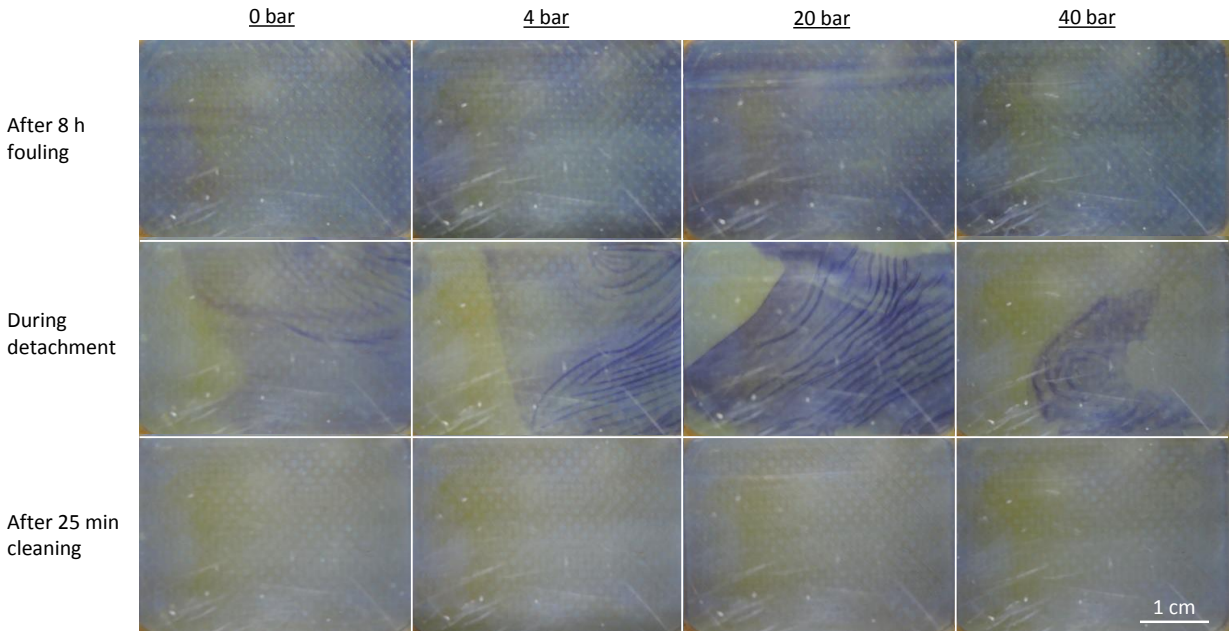

Figure 12: Stills from video of cleaning FO membranes fouled with low-salinity feed (29 mM NaCl, 1 mM $CaCl_2$, 200 mg/L alginate, and 7.4 μM methylene blue). In each case, the sheet of gel detached from the membrane and was swept away in the flow (left to right).

here. However, the video reveals no clear difference between cleaning processes at 0 and 30 bar; in either case, small pieces of gel detach and flow along the direction of one set of spacer filaments. After cleaning, many pieces of gel remain in the channel. These recordings do not support previous assertions that unpressurized alginate gel is more susceptible to breakup by shear stress.

5. Discussion: fouling resistance in FO

Although high feed pressure is often blamed for the difficulty of removing fouling in RO, this study provides evidence that feed hydraulic pressure does not affect fouling or foulant removal. No effect of feed pressure on flux decline was observed, and there was no clear relationship between feed pressure and cleaning effectiveness. Furthermore, in situ visualization of the cleaning process demonstrated that the mechanisms of fouling removal did not vary with feed pressure. The effect of pressure on fouling identified in this study

likely differs from previous findings due to the variation of draw pressure, rather than draw concentration, to maintain initial flux across trials at different feed pressures.

Significant differences found by previous studies in cleaning effectiveness after fouling at different feed pressures and draw solution concentrations could have been influenced by either the draw solutions or effects of TMP on the membrane. This section discusses three possible causes for the difference in fouling propensity between RO and FO that are unrelated to foulant compaction by high feed pressure. Future research should explore these and other possible explanations, identify the cause of high organic fouling reversibility in FO, and use this knowledge to enhance the fouling resistance of FO. Because this study has shown that low pressure is not necessary for high fouling resistance, it is possible that the cause of FO's fouling resistance can also be adapted to improve the fouling resistance of RO.

5.1. TMP

It is possible that TMP could have affected fouling reversibility in previous studies for reasons unrelated to foulant compaction. Without high TMP pressing a membrane against a permeate carrier, a fouled FO membrane has the potential to move around during cleaning. Membrane vibration has been used to remove fouling from RO membranes [42], so it is possible that FO membrane movement during normal cleaning could similarly enhance foulant removal. Additionally, applying TMP increases membrane roughness, as is apparent in SEM and CLSM images of fouled FO membranes used with and without TMP [22]. Increasing membrane roughness raises the contact area between foulant and membrane, and could potentially hinder foulant removal.

5.2. Solute back-diffusion

Diffusion of NaCl from the draw solution to the feed, which can significantly affect cake layer ion concentration [7, 17], may lead to differences in gel properties between FO and RO tests with alginate fouling and a draw solution of NaCl due to the ion exchange

reaction between sodium and calcium ions in alginate gels [43]. LeRoux et al. [44] measured compressive and shear moduli of alginate gels in calcium chloride solutions with and without sodium chloride and found that compressive and shear moduli decrease by 63% and 84%, respectively, due to the addition of 0.15 M sodium chloride. However, a difference in cleaning effectiveness between FO and RO has been observed even with a glucose draw solution [15], so NaCl back-diffusion alone cannot explain the disparity in fouling reversibility observed between FO and RO.

5.3. ICP and foulant heterogeneity

Fouling layers formed in FO tend to be more bumpy than those formed in RO. CLSM images show spatial heterogeneity in foulant thickness of both alginate fouling [15] and *Pseudomonas aeruginosa* biofouling [22] in FO alongside uniform-thickness layers formed in RO on the same membrane under identical hydrodynamic conditions. Optical micrographs of latex particle deposition on FO membranes (refer to Fig. 2b in [45]) also show a pattern of heterogeneous particle deposition that has gaps where the membrane's support mesh filaments cross.

Foulant layer heterogeneity in FO could potentially result from spatially-varying local flux. Spatial variations in FO membrane support layer mass transfer resistance may occur due to the heterogeneous pore structure and, where present, the embedded support mesh. In FO, the local transmembrane flux will be smaller where the support layer mass transfer resistance is greater (e.g., where two mesh filaments cross). When the same membrane is used in RO, the hydraulic resistance of the support layer is negligible relative to the resistance to flow through the active layer, and the local flux depends only on the properties of the active layer. Because of the significant influence of the support layer on flux in FO, the same membrane may have greater spatial variation in flux when used in FO than in RO. Higher local flux leads to greater convection of foulants (and, in the case of biofouling, nutrients) to

the membrane and a locally thicker fouling layer. The potential for higher spatial variation in flux in FO may explain the observed heterogeneity of fouling layers formed in FO.

Fouling layer heterogeneity has the potential to affect ease of removal in several ways. A foulant layer with some thinner regions may break up more easily. Increased foulant layer roughness may allow high-velocity feed flow to create more lift. Variations in foulant layer thickness may create regions of stress concentration when the foulant layer swells or shrinks (e.g., due to changing ion concentration [16]) during a cleaning procedure, which may hasten detachment from the membrane. Further study is required to determine whether these proposed mechanisms have a significant effect on foulant removal.

6. Conclusion

The effect of foulant compression on flux decline depends on the foulant cake pore size and feed osmotic pressure. According to the model developed here, compression of alginate foulant layers would be expected to increase the rate of flux decline at low salinity; however, at high salinity, compression would be expected to retard flux decline by reducing cake-enhanced concentration polarization. These predictions were used to interpret the results of FO fouling experiments with both feed and draw streams at elevated pressure and determine the role of hydraulic pressure on fouling.

Higher hydraulic pressure did not result in the more rapid flux decline that was expected of compressible gels at the low feed salinity tested. In contrast to the trend identified by previous studies, which varied feed pressure and draw solution concentration together, the present study showed no effect of feed hydraulic pressure on cleaning effectiveness. Furthermore, in situ visualization revealed no difference in foulant removal mechanisms over the range of pressures tested (0–40 bar). These results do not support the prevalent theory that high feed pressure compacts foulants and impedes membrane cleaning in RO.

Based on these results, foulant compaction by high pressure should no longer be consid-

ered the cause of the high fouling propensity of RO relative to FO. Several other differences between FO and RO may be responsible for the difference in these systems' fouling propensity. Future research should aim to pinpoint the cause of FO's fouling resistance and to apply this knowledge to improving the fouling resistance of both FO and RO desalination systems.

7. Acknowledgment

EWT would like to acknowledge support from the Martin Fellowship for Sustainability. This material is based upon work supported by the National Science Foundation Graduate Research Fellowship Program under Grant No. 1122374. Partial support from the King Fahd University of Petroleum and Minerals through the Center for Clean Water and Clean Energy at MIT and KFUPM (Project #R4-CW-11) is gratefully acknowledged. We thank Prof. Lallit Anand for useful discussions.

References

[1] R. L. McGinnis, M. Elimelech, Energy requirements of ammonia–carbon dioxide forward osmosis desalination, Desalination 207 (2007) 370–382. http://dx.doi.org/10.1016/j.desal.2006.08.012.

[2] R. Semiat, Energy issues in desalination processes, Environmental Science & Technology 42 (2008) 8193–8201. http://dx.doi.org/10.1021/es801330u.

[3] R. K. McGovern, J. H. Lienhard V, On the potential of forward osmosis to energetically outperform reverse osmosis desalination, Journal of Membrane Science 469 (2014) 245–250. http://dx.doi.org/10.1016/j.memsci.2014.05.061.

[4] D. L. Shaffer, J. R. Werber, H. Jaramillo, S. Lin, M. Elimelech, Forward osmosis: Where are we now?, Desalination 356 (2015) 271–284. http://dx.doi.org/10.1016/j.desal.2014.10.031.

[5] G. P. Thiel, E. W. Tow, L. D. Banchik, H. W. Chung, J. H. Lienhard V, Energy consumption in desalinating produced water from shale oil and gas extraction, Desalination 366 (2015) 94–112. http://dx.doi.org/10.1016/j.desal.2014.12.038.

[6] E. W. Tow, R. K. McGovern, J. H. Lienhard V, Raising forward osmosis brine concentration efficiency through flow rate optimization, Desalination 366 (2015) 71–79. http://dx.doi.org/10.1016/j.desal.2014.10.034.

[7] S. Lee, C. Boo, M. Elimelech, S. Hong, Comparison of fouling behavior in forward osmosis (FO) and reverse osmosis (RO), Journal of Membrane Science 365 (2010) 34–39. http://dx.doi.org/10.1016/j.memsci.2010.08.036.

[8] B. Mi, M. Elimelech, Organic fouling of forward osmosis membranes: Fouling reversibility and cleaning without chemical reagents, Journal of Membrane Science 348 (2010) 337–345. http://dx.doi.org/10.1016/j.memsci.2009.11.021.

[9] Y. Chun, F. Zaviska, S.-J. Kim, D. Mulcahy, E. Yang, I. S. Kim, L. Zou, Fouling characteristics and their implications on cleaning of a FO-RO pilot process for treating brackish surface water, Desalination 394 (2016) 91–100. http://dx.doi.org/10.1016/j.desal.2016.04.026.

[10] B. Mi, M. Elimelech, Chemical and physical aspects of organic fouling of forward osmosis membranes, Journal of Membrane Science 320 (2008) 292–302. http://dx.doi.org/10.1016/j.memsci.2008.04.036.

[11] C. Boo, M. Elimelech, S. Hong, Fouling control in a forward osmosis process integrating seawater desalination and wastewater reclamation, Journal of Membrane Science 444 (2013) 148–156. http://dx.doi.org/10.1016/j.memsci.2013.05.004.

[12] R. W. Holloway, A. E. Childress, K. E. Dennett, T. Y. Cath, Forward osmosis for concentration of anaerobic digester centrate, Water Research 41 (2007) 4005–4014. http://dx.doi.org/10.1016/j.watres.2007.05.054.

[13] G. Qiu, Y.-P. Ting, Short-term fouling propensity and flux behavior in an osmotic membrane bioreactor for wastewater treatment, Desalination 332 (2014) 91–99. http://dx.doi.org/10.1016/j.desal.2013.11.010.

[14] Y. Kim, M. Elimelech, H. K. Shon, S. Hong, Combined organic and colloidal fouling in forward osmosis: Fouling reversibility and the role of applied pressure, Journal of Membrane Science 460 (2014) 206–212. http://dx.doi.org/10.1016/j.memsci.2014.02.038.

[15] M. Xie, J. Lee, L. D. Nghiem, M. Elimelech, Role of pressure in organic fouling in forward osmosis and reverse osmosis, Journal of Membrane Science 493 (2015) 748–754. http://dx.doi.org/10.1016/j.memsci.2015.07.033.

[16] E. W. Tow, M. M. Rencken, J. H. Lienhard V, In situ visualization of organic fouling and cleaning mechanisms in reverse osmosis and forward osmosis, Desalination 399 (2016) 138–147.

http://dx.doi.org/10.1016/j.desal.2016.08.024.

[17] W. C. L. Lay, C. Tzyy Haur, C. Y. Tang, A. G. Fane, Z. Jinsong, L. Yu, Fouling propensity of forward osmosis: investigation of the slower flux decline phenomenon., Water Science & Technology 61 (2010) 927–936. http://dx.doi.org/10.2166/wst.2010.835.

[18] Q. She, R. Wang, A. G. Fane, C. Y. Tang, Membrane fouling in osmotically driven membrane processes: A review, Journal of Membrane Science 499 (2016) 201 –233. http://dx.doi.org/10.1016/j.memsci.2015.10.040.

[19] E. W. Tow, J. H. Lienhard V, Quantifying osmotic membrane fouling to enable comparisons across diverse processes, Journal of Membrane Science 511 (2016) 92–107. http://dx.doi.org/10.1016/j.memsci.2016.03.040.

[20] E. R. Morris, D. A. Rees, D. Thom, J. Boyd, Chiroptical and stoichiometric evidence of a specific, primary dimerisation process in alginate gelation, Carbohydrate Research 66 (1978) 145–154. http://dx.doi.org/10.1016/S0008-6215(00)83247-4.

[21] I. Braccini, S. Perez, Molecular basis of Ca^{2+}-induced gelation in alginates and pectins: The egg-box model revisited, Biomacromolecules 2 (2001) 1089–1096. http://dx.doi.org/10.1021/bm010008g.

[22] S. E. Kwan, E. Bar-Zeev, M. Elimelech, Biofouling in forward osmosis and reverse osmosis: Measurements and mechanisms, Journal of Membrane Science 493 (2015) 703–708. http://dx.doi.org/10.1016/j.memsci.2015.07.027.

[23] S. T. Moe, G. Skjaak-Braek, A. Elgsaeter, O. Smidsrod, Swelling of covalently crosslinked alginate gels: influence of ionic solutes and nonpolar solvents, Macromolecules 26 (1993) 3589–3597. http://dx.doi.org/10.1021/ma00066a017.

[24] R. W. Field, D. Wu, J. A. Howell, B. B. Gupta, Critical flux concept for microfiltration fouling, Journal of Membrane Science 100 (1995) 259–272. http://dx.doi.org/10.1016/0376-7388(94)00265-Z.

[25] A. Karabelas, D. Sioutopoulos, New insights into organic gel fouling of reverse osmosis desalination membranes, Desalination 368 (2015) 114–126. http://dx.doi.org/10.1016/j.desal.2015.01.029.

[26] C. Wang, C. Cowen, Z. Zhang, C. Thomas, High-speed compression of single alginate microspheres, Chemical Engineering Science 60 (2005) 6649–6657. http://dx.doi.org/10.1016/j.ces.2005.05.052.

[27] A. S. Argon, S. Backer, F. A. McClintock, G. S. Reichenbach, E. Orowan, M. C. Shaw, E. Rabinowicz, Mechanical Behavior of Materials, Addison-Wesley Publishing Company, Inc., 1966.

[28] T. Fujioka, N. Oshima, R. Suzuki, W. E. Price, L. D. Nghiem, Probing the internal structure of reverse osmosis membranes by positron annihilation spectroscopy: Gaining more insight

into the transport of water and small solutes, Journal of Membrane Science 486 (2015) 106–118. http://dx.doi.org/10.1016/j.memsci.2015.02.007.

[29] D. Cohen-Tanugi, J. C. Grossman, Water desalination across nanoporous graphene, Nano Letters 12 (2012) 3602–3608. http://dx.doi.org/10.1021/nl3012853.

[30] J. Wijmans, R. Baker, The solution-diffusion model: a review, Journal of Membrane Science 107 (1995) 1–21. http://dx.doi.org/10.1016/0376-7388(95)00102-I.

[31] D. R. Paul, Reformulation of the solution-diffusion theory of reverse osmosis, Journal of Membrane Science 241 (2004) 371–386. http://dx.doi.org/10.1016/j.memsci.2004.05.026.

[32] D. R. Paul, The role of membrane pressure in reverse osmosis, Journal of Applied Polymer Science 16 (1972) 771–782. http://dx.doi.org/10.1002/app.1972.070160320.

[33] Y. Ye, P. Le Clech, V. Chen, A. G. Fane, B. Jefferson, Fouling mechanisms of alginate solutions as model extracellular polymeric substances, Desalination 175 (2005) 7–20. http://dx.doi.org/10.1016/j.desal.2004.09.019.

[34] H.-C. Flemming, T. R. Neu, J. Wingender, The Perfect Slime: Microbial Extracellular Polymeric Substances (EPS), IWA Publishing, 2016.

[35] B. Ghanbarian, A. G. Hunt, R. P. Ewing, M. Sahimi, Tortuosity in porous media: A critical review, Soil Science Society of America Journal 77 (2013) 1461–1477. http://dx.doi.org/10.2136/sssaj2012.0435.

[36] E. Mauret, M. Renaud, Transport phenomena in multi-particle systems–I. Limits of applicability of capillary model in high voidage beds-application to fixed beds of fibers and fluidized beds of spheres, Chemical Engineering Science 52 (1997) 1807–1817. http://dx.doi.org/10.1016/S0009-2509(96)00499-X.

[37] E. M. V. Hoek, M. Elimelech, Cake-enhanced concentration polarization: A new fouling mechanism for salt-rejecting membranes, Environmental Science and Technology 37 (2003) 5581–5588. http://dx.doi.org/10.1021/es0262636.

[38] B. A. Qureshi, S. M. Zubair, A. K. Sheikh, A. Bhujle, S. Dubowsky, Design and performance evaluation of reverse osmosis desalination systems: An emphasis on fouling modeling, Applied Thermal Engineering 60 (2013) 208–217. http://dx.doi.org/10.1016/j.applthermaleng.2013.06.058.

[39] J. S. Ho, L. N. Sim, J. Gu, R. D. Webster, A. G. Fane, H. G. Coster, A threshold flux phenomenon for colloidal fouling in reverse osmosis characterized by transmembrane pressure and electrical impedance spectroscopy, Journal of Membrane Science 500 (2016) 55–65. http://dx.doi.org/10.1016/j.memsci.2015.11.006.

[40] O. Smidsrod, Molecular basis for some physical properties of alginates in the gel state, Faraday

Discussions of the Chemical Society 57 (1974) 263–274. http://dx.doi.org/10.1039/DC9745700263.

[41] E. W. Tow, J. H. Lienhard V, Effect of pressure on alginate fouling in forward osmosis, in: AMTA/AWWA Membrane Technology Conference, Long Beach, CA, USA, Feb. 13-17.

[42] B. Liberman, I. Liberman, Forward osmotic and water hammer method of membrane cleaning, 2016. WO Patent App. PCT/IB2015/055,665.

[43] O. Smidsrod, A. Haug, The effect of divalent metals on the properties of alginate solutions: I. Calcium ions, Acta Chemica Scandinavica 19 (1965) 329–340. http://actachemscand.org/pdf/acta_vol_19_p0329-0340.pdf.

[44] M. A. LeRoux, F. Guilak, L. A. Setton, Compressive and shear properties of alginate gel: Effects of sodium ions and alginate concentration, Journal of Biomedical Materials Research 47 (1999) 46–53. http://dx.doi.org/10.1002/(SICI)1097-4636(199910)47:1¡46::AID-JBM6¿3.0.CO;2-N.

[45] Y. Wang, F. Wicaksana, C. Y. Tang, A. G. Fane, Direct microscopic observation of forward osmosis membrane fouling, Environmental Science & Technology 44 (2010) 7102–7109. http://dx.doi.org/10.1021/es101966m.

[46] S. Lee, M. Elimelech, Salt cleaning of organic-fouled reverse osmosis membranes, Water Research 41 (2007) 1134–1142. http://dx.doi.org/10.1016/j.watres.2006.11.043.

[47] T. G. Beckwith, R. D. Marangoni, J. H. Lienhard V, Mechanical Measurements, 6th edition, Pearson, 2007.

Appendix A. Effect of pressure on unfouled membrane performance

Permeability varied significantly between membrane coupons, particularly those cut from different sheets, causing variability in initial flux. Each trial began with near-saturated NaCl draw solutions whose variation in concentration should lead to initial fluxes within approximately ± 0.75 lmh if all membrane samples had identical properties, according to the FO membrane transport model of Ref. [19]. However, the actual initial fluxes varied ± 5.7 lmh, suggesting a significant variation in membrane properties between coupons. To show that apparent effects of initial flux on flux decline rate are not related to hydraulic pressure through any effect of hydraulic pressure on initial flux, initial flux before fouling is plotted versus hydraulic pressure in Fig. A.13. The lack of dependence of initial flux on

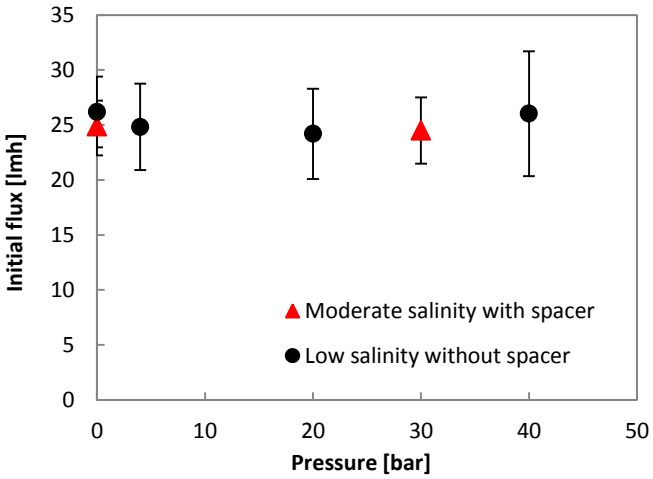

Figure A.13: Initial flux before fouling for all experimental trials.

pressure is further demonstrated by near-zero correlation coefficients between pressure and initial flux of 0.02 and -0.08 for the low-salinity and moderate-salinity trials, respectively.

Appendix B. Cleaning effectiveness

The removal of foulant from the FO membrane by cleaning (using the protocol described in Sec. 3.3) is represented by a cleaning effectiveness, ϵ_c, which is calculated from the change in normalized flux due to cleaning as defined in Eq. B.1:

$$\epsilon_c = \frac{J_a/J_{a,0} - J_b/J_{b,0}}{1 - J_b/J_{b,0}}, \tag{B.1}$$

where J is the water flux, the subscript 0 refers to the foulant-free flux prediction, and the subscripts b and a refer to before and after cleaning, respectively. Similar definitions have been used in previous studies to quantify the recovery of flux by cleaning [15, 46]. Permeate flow between 15 and 30 minutes after the conclusion of the cleaning step is used in calculating flux after cleaning and cleaning effectiveness. The uncertainty in cleaning effectiveness is discussed in Appendix C.

Appendix C. Uncertainty analysis

Using the method of propagation of uncertainty (see [47]) and the definition of cleaning effectiveness (Eq. B.1), the uncertainty (as a 95% confidence interval) in cleaning effectiveness, u_{ϵ_c}, can be expressed in terms of uncertainties in normalized flux before and after cleaning:

$$u_{\epsilon_c} = \sqrt{\left(u_{(J_a/J_{a,0})}\frac{\partial \epsilon_c}{\partial (J_a/J_{a,0})}\right)^2 + \left(u_{(J_b/J_{b,0})}\frac{\partial \epsilon_c}{\partial (J_b/J_{b,0})}\right)^2}. \tag{C.1}$$

Reference [19] showed that the 95% confidence interval in normalized FO flux for the present apparatus was approximately ± 0.04. Using this value for uncertainty in normalized flux both before and after cleaning ($u_{(J_a/J_{a,0})} = u_{(J_b/J_{b,0})} = 0.04$), and evaluating derivatives based on Eq. B.1:

$$\frac{\partial \epsilon_c}{\partial (J_a/J_{a,0})} = \frac{1}{1 - J_b/J_{b,0}} \tag{C.2}$$

and

$$\frac{\partial \epsilon_c}{\partial (J_b/J_{b,0})} = \frac{1 - J_a/J_{a,0}}{(1 - J_b/J_{b,0})^2}, \tag{C.3}$$

the 95% confidence interval in cleaning effectiveness can be estimated by Eq. C.4:

$$u_\epsilon = \frac{0.04}{1 - J_b/J_{b,0}}\sqrt{1 + \left(\frac{1 - J_a/J_{a,0}}{1 - J_b/J_{b,0}}\right)^2}. \tag{C.4}$$